RSC Advances

PAPER

View Article Online
View Journal | View Issue



Cite this: *RSC Adv.*, 2015, **5**, 14974

# Mechanism of photoluminescence enhancement and quenching in $Nd_2O_3$ nanoparticles–ferroelectric liquid crystal nanocomposites

Puja Goel*[a] and Manju Arora[b]

Received 10th November 2014
Accepted 19th January 2015

DOI: 10.1039/c4ra14204g

www.rsc.org/advances

The mechanism of photoluminescence enhancement and quenching in np-$Nd_2O_3$:FLC nanocomposites has been explored in the current study by UV-Vis and photoluminescence (PL) spectroscopy techniques. UV-Vis absorption spectra of $Nd_2O_3$ NPs in the 200–800 nm range shows two absorptions at 248 nm and 292 nm whereas pure FLC gives a broad absorption in the 265 nm to 348 nm region. PL emission intensity of np-$Nd_2O_3$:FLC composites recorded at 248 nm excitation wavelength where $Nd_2O_3$ NPs show intense emission, increases with gradually increasing the concentration of NPs up to 8 μl. This enhancement in PL intensity without blue/red shifting the FLC's emission band was attributed to the up-conversion of doped $Nd^{3+}$ ions and transfer of excitation energy to liquid crystal molecules. When excited with 248 nm, the $Nd^{3+}$ ground state $^4I_{9/2}$ absorption excites electrons to a higher excited state $^2G_{5/2}$. The excited $Nd^{3+}$ ions in $^2G_{5/2}$ level relax non-radiatively to the metastable $^2H_{11/2}$ state and then re-excites to an unstable $^4G_{11/2}$ level. The electrons populated in $^4G_{11/2}$ release energy either radiatively to different defect energy levels in the visible region or transfers this excitation energy to liquid crystal molecules which resulted into the enhancement in PL emission intensity. On the other hand, emission spectra at 303, 323, 333, 343 nm excitation wavelengths exhibit quenching of all emission bands in np-$Nd_2O_3$:FLC composites due to the stress induced structural disordering by the $Nd_2O_3$ NPs in the FLC matrix and creation of non-radiative channels in the system.

## Introduction

Research in the field of nanoparticle (NP) doped liquid crystal materials has increased exponentially due to the combination of two recent active areas of nanoscience and liquid crystals (LCs). The nanomaterial dispersed LCs have enormous industrial applications in the fabrication of better contrast luminescent liquid crystal based displays and optoelectronic devices as compared to earlier reported aerosil particle dispersed FLCs.[1–6] As of today, liquid crystals are an indispensible component of modern display technology and they have also acquired a very important place in various non-display devices such as optical storage and optical switching owing to their unique ability of reorienting the electric polarization. Recently, research on FLCs doped with metal nanoparticles (MNPs) and metal oxide nanoparticles (MONPs) reported the improvement in various physical properties like electro-optic, magneto-optic, dielectric, conductivity and luminescent behaviour of these colloids.[7–12] The coupling of quantum dots of various nanoscale materials with LCs further encourages their use in the development of new potential applications which are yet under investigation or to be explored.

The optical properties of FLCs doped analogues with dopants like dispersion of nobel metal gold, silver, platinum of size ~5 nm and palladium NPs,[13–15] barium titanate ($BaTiO_3$) NPs,[16] rare earth oxide nano-ceria[17] and ZnO/ZnS quantum dots[18] *etc.* have been studied by electro-optic and photoluminescence (PL) spectroscopy. Recently T. Lahiri *et al.*[19] developed a theory for the statistical mechanics of NPs doped in FLC by assuming that the NPs in FLC medium creates strong local fields that produce large alignment effects over the distribution of the nanosuspensions. The enhancement in PL peak intensity has been discussed in terms of the coupling of localized surface plasmon resonance from MNPs with distorted helical FLC molecules.[15] The increase in intensity of PL absorption was nine folds in gold NPs doped distorted FLC while two folds increase was reported in 0.2 wt% $BaTiO_3$ doped FLC. The coupling of large dipole moment of ferroelectric $BaTiO_3$ with FLC induces increase in PL intensity. Kumar *et al.*[18] reported photoluminescence phenomenon in a deformed helix FLC due to presence of optically active phenyl pyrimidine compound which is an electroluminescent material. Hence, these studies are the benchmark for realization of high luminescent next generation FLC devices with fast response.

[a]*Division of Agricultural Chemicals, Indian Agricultural Research Institute, New Delhi 110012, India. E-mail: pujagoel@gmail.com*

[b]*CSIR – National Physical Laboratory, Dr K. S. Krishnan Marg, New Delhi 110012, India*

Rare earth compounds have unique properties and wide uses owing to their special electronic configuration. The efficient multicolour luminescence of rare earth ions has been utilized in light emitting diodes (LEDs) and lasers.[20,21] The host sensitization through energy transfer from the excited host to rare earth ions is an effective way to restrict the parity-forbidden f–f transitions. The luminescence of rare earth ions is markedly improved by non-radiative energy transfer from the triplet state of ligands to the crystal-field of the metal ions in metal organic complexes. Among rare earth metal ions, neodymium ion is used as a luminescent centre in laser systems due to its four-level energy structure. The band gap energy of $Nd_2O_3$ nanoparticles lies in the range from 5.25 eV to 5.70 eV. The possibility of obtaining UV, blue, green and red luminescence in the PL emission of $Nd_2O_3$ NPs at different excitation wavelengths has emerged the importance of these NPs as high performance optical materials in various optical device applications. Taking this in to consideration, we have dispersed varied amount of $Nd_2O_3$ NPs suspension in FLC and characterized their FTIR, UV-Vis and photoluminescence response in terms of varying NPs concentration and wavelength of excitation.

## Experimental

For current studies, electro-optic cells of thickness 4 μm were procured from INSTEC USA. These cells consisted of square patterned transparent and conducting (30 Ω $cm^{-2}$) indium tin oxide (ITO) coated optically flat glass substrates coated with a polymer to entail a 180° (homogeneous) alignment of liquid crystal layers over substrates.

In order to make np-$Nd_2O_3$:FLC nanocomposites, first of all a suspension of $Nd_2O_3$ NPs was prepared in double distilled water. For suspension preparation, 0.001 g of $Nd_2O_3$ NPs were mixed in 100 ml of double distilled water and ultrasonicated for 1 h. Selective amounts of this suspension (*i.e.* 2, 3, 5 and 8 μl of suspension) were added to a fix quantity of (4 mg) of FLC material. All these mixtures were rigorously mixed to ensure homogenous dispersion of NPs among FLC. Mixing process was followed by repeated heating at 110 °C for complete evaporation of water content before inserting the mixtures in to electro-optic cells. Phase sequence of investigated FLC *i.e.*, ZLi 3654 is as follows:

$$\text{Cryst.} \xleftrightarrow{-30\ ^\circ\text{C}} \text{SmC*} \xleftrightarrow{62\ ^\circ\text{C}} \text{SmA*} \xleftrightarrow{76\ ^\circ\text{C}} \text{N*} \xleftrightarrow{86\ ^\circ\text{C}} \text{Iso.}$$

where Cryst., SmC*, SmA*, N*, and Iso. denotes crystal, chiral smectic C, chiral smectic A, chiral nematic and isotropic phases respectively.

To establish the size and phase purity of NPs, X-ray diffraction spectra of NPs was recorded by using X-ray diffractometer (XRD, Bruker D8 Advance) using CuKα radiation ($\lambda = 1.5414$ Å). Transmission Electron Microscopy (TEM) studies were also conducted to check the size of nanoparticles and their size distribution using JEOL-JEM (1011) microscope. In order to ascertain the optical quality of nanocomposites, optical micrographs of the pure as well as NPs dispersed samples were first checked with the help of a polarising optical microscope (Ax-40, Carl Zeiss, Gottingen, Germany). Further, to study the molecular director change of FLC after NPs doping and to see the interaction between NPs and FLC, transmission FTIR spectra were recorded using FTIR ALPHA T (Bruker) instrument at room temperature. UV-Vis absorption spectrum of NPs and FLC was recorded using Shimadzu UV-Vis spectrophotometer (model no. UV-2401 PV) in 200 nm–800 nm range. The photoluminescence spectra (PL) of pure and $Nd_2O_3$ dispersed samples were recorded on a Fluorolog (JobinYvon–Horiba, model-3-11) spectrofluorometer.

## Results and discussion

Fig. 1 shows the XRD pattern of $Nd_2O_3$ NPs which confirmed phase pure hexagonal $Nd_2O_3$ NPs (JCPDS card no. 41-1089) without any impurity phases. Particle size was estimated using Scherrer's equation[22]

$$P = \frac{k\lambda}{\beta_{1/2}\cos\theta}$$

where $k = 0.89$ is a constant, $\theta$ is Bragg's angle and $\beta_{1/2}$ is full-width at half maximum (FWHM) intensity. Estimated particle size was found to be 50 nm which is in accordance with the size claimed (<100 nm) by supplier (Sigma Aldrich). TEM images of nanoparticles in Fig. 2(a) exhibit the spherical shaped NPs with estimated size in the range of $\sim 15 \pm 2$ nm. Due to small crystallite size, the surface activity of these particles arising from large surface area to volume ratio is very high which encourages the agglomeration and stabilization of particles by forming clusters of spherical shaped particles. Size distribution of NPs, estimated from an average of 200 number of particles as seen in TEM image, has been depicted through the histogram in Fig. 2(b) and can be well fitted by the log normal distribution function[17]

$$y = y_0 + \frac{A}{w \times x\sqrt{2\pi}} \exp\left(-\frac{(\ln(x/x_c))^2}{2 \times w^2}\right)$$

where "$w$" represents the standard deviation and "$x_c$" is the mean particle size. Further, to check the optical quality of np-$Nd_2O_3$:FLC nanocomposites, textures of samples were

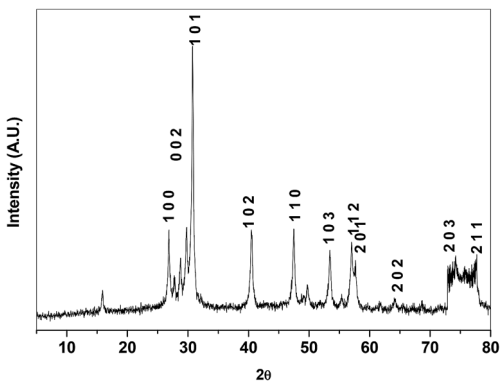


Fig. 1 XRD pattern of $Nd_2O_3$ Nanoparticles.

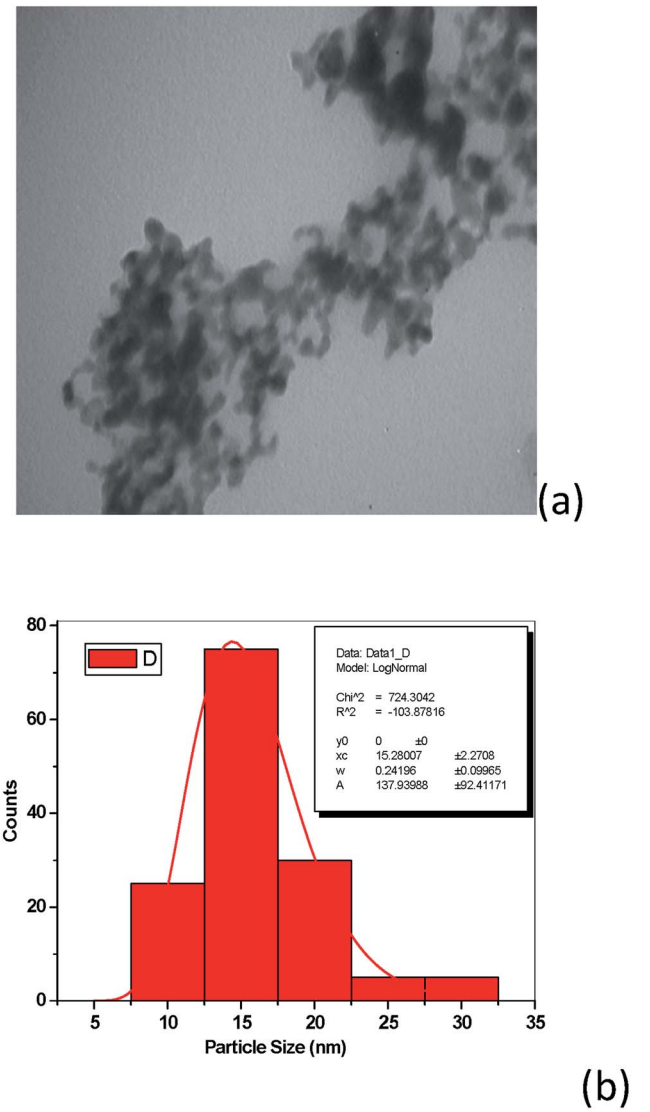


Fig. 2 (a) TEM image of the $Nd_2O_3$ NPs (b) particle size distribution histogram ($w$ is standard deviation and $x_c$ represents mean particle size ~15 ± 2 nm).

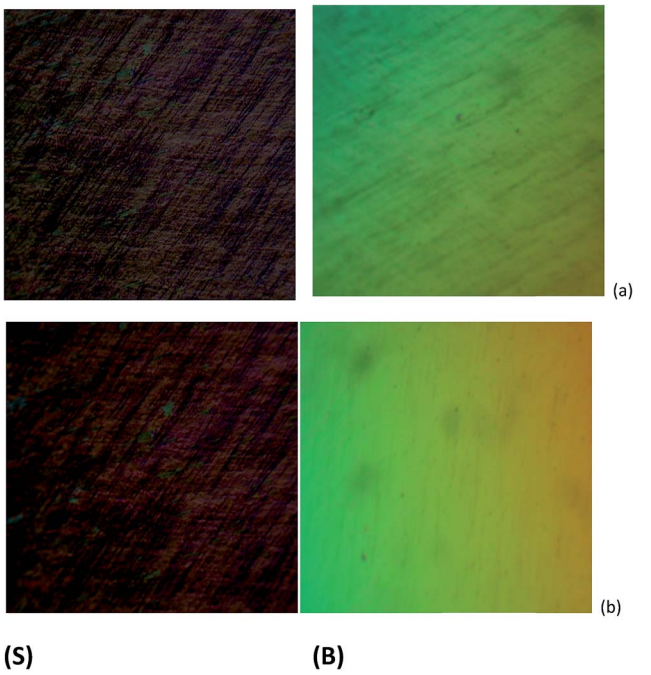


Fig. 3 Polarising optical micrographs of (a) FLC (ZLi 3654) (b) 8 μl $Nd_2O_3$ NPs dispersed FLC (ZLi 3654) (S) denote 'scattered/dark' and (B) denote "Bright" states respectively.

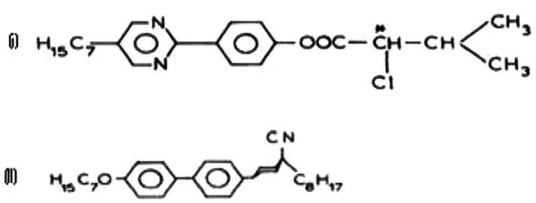

The peaks pertaining to –C≡N stretch. vibration (2231 $cm^{-1}$), –C=C– aromatic ring vibration (1585 $cm^{-1}$), –C=N ring stretch. mode (1542 $cm^{-1}$), $CH_2$ asym. bend. mode (1499 $cm^{-1}$), C–H out-of-plane bend. (822 $cm^{-1}$), –C–Cl out-of-plane bending mode (798 $cm^{-1}$), C–H out-of-plane bend. (759 $cm^{-1}$), out-of-plane –C=C– ring bend. (654 $cm^{-1}$) remains unaltered in presence of $Nd_2O_3$ NPs whereas a small shift of 1–4 $cm^{-1}$ is observed in the bands corresponding to the out-of-plane C–C–Cl bend. mode, O=C=C asym. stretch. mode, $CH_3$ sym. and asym. bend. mode, $CH_2$ sym. bend. mode, C–H stretch. mode of $CH_3$ and $CH_2$ groups. C–H stretching and symmetric bending mode of $CH_2$ group shifts from 2932 $cm^{-1}$ and 1378 $cm^{-1}$ (FLC) to 2928 $cm^{-1}$ and 1375 $cm^{-1}$ ($Nd_2O_3$ NPs:FLC) respectively. $CH_3$ symmetric bending mode is observed at 1328 $cm^{-1}$ in FLC and shift to 1326 $cm^{-1}$ in NPs dispersed FLC. On the other hand, in-plane OH bonded aromatic ring bending mode and hydrogen bonded in-plane OH bending of aromatic ester are obtained at 1300 and 1111 $cm^{-1}$ respectively in FLC and these peaks shift to 1303 to 1115 $cm^{-1}$ in np-$Nd_2O_3$:FLC nanocomposites. This confirms that the NPs are interacting with the long terminal alkyl groups of aromatic cored liquid crystal molecules whereas inner core remains unaffected. The shift in the peak position to low wavenumbers

analyzed under polarizing microscope and it has been found that alignment of liquid crystal molecule did not get disturbed in presence of $Nd_2O_3$ NPs even in the maximum concentration (8 μl) used in the present study (Fig. 3).

FTIR spectroscopy has been used for the detection of vibrational characteristics of functional groups present in FLC and $Nd_2O_3$ nanoparticles dispersed FLC samples. IR transmission spectra of pure FLC, $Nd_2O_3$ nanoparticles (NPs) and NPs dispersed FLC composites recorded in 4000–500 $cm^{-1}$ region at ambient temperature are presented in Fig. 4(a)–(c) respectively. Since this ferroelectric LC mixture consisted of two compounds with following structural formulas, various vibrational bands are possible corresponding to the central aromatic core and aliphatic terminal groups These spectra show characteristic peaks of –C≡N, –C–Cl, –COO, $–CH_2$, $–CH_3$ and –C=C– aromatic ring vibration of FLC and Nd–O stretching modes.[23–27]

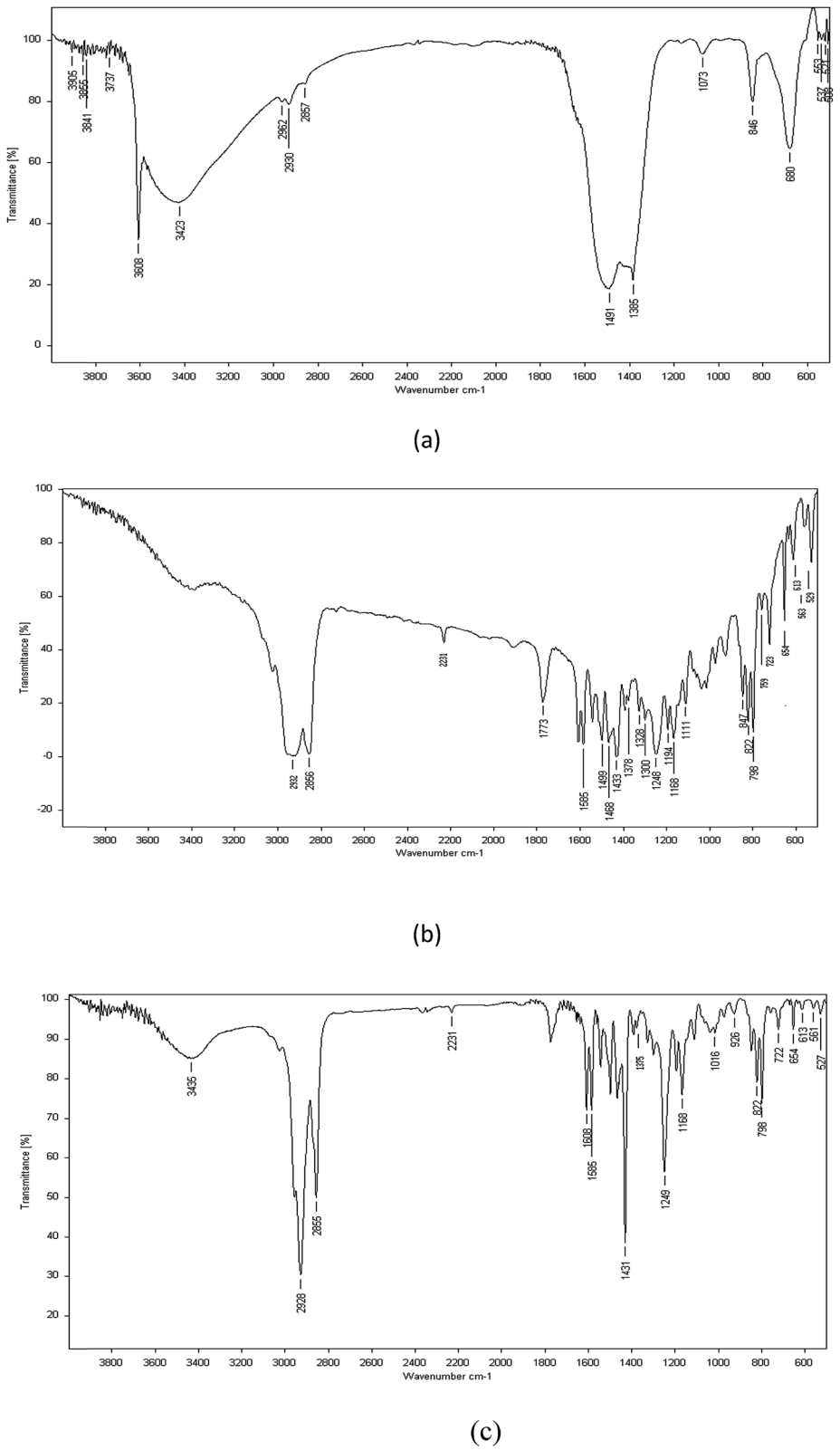


Fig. 4 FTIR spectra of the (a) $Nd_2O_3$ NPs, (b) FLC mixture and (c) 2 μl $Nd_2O_3$ NPs dispersed FLC.

with change in intensity reveals that $Nd_2O_3$ NPs are weakly bonded to FLC alkyl chains by hydrogen bonding. While aromatic core bonded ester carbonyl (O–C═O) and its hydrogen bonded (C═O···H) groups are strained and appear at higher wavenumbers due to interstitial site substitution of NPs in FLC matrix. The appearance of Nd–O stretch. mode at 680 $cm^{-1}$ in

np-$Nd_2O_3$:FLC further confirms the incorporation of NPs in FLC matrix and their interaction with FLC molecules.

Optical absorption and emission properties of nanocomposites have been investigated by means of ultraviolet-visible spectrophotometry and photoluminescence spectroscopy. In order to find the desired excitation wavelength for PL measurement, UV-Visible absorption spectra of $Nd_2O_3$ NPs and FLC mixture were recorded in 200–800 nm region. As the optimal wavelength for excitation corresponds to the maximum of absorption spectrum, the PL spectrum were recorded at the energy (corresponding wavelength) greater than or equal to the value of band gap energy estimated from UV-Vis spectrum.

As demonstrated in Fig. 5(a), UV-Vis absorption spectra of $Nd_2O_3$ NPs (~50 nm size) in 200–800 nm range shows two absorptions at 248 and 292 nm with a tail of the absorption extending well in the visible region (*i.e.* upto 800 nm). The hump around 248 nm appears to be more prominent as compared to the 292 nm absorption. The calculated band gap energy for $Nd_2O_3$ NPs ranges from 4.2 eV–4.98 eV due to variation in particle size because the highly active nanoparticles have large surface to volume ratio and have tendency to form voids on the surface as well as inside the agglomerated particles. These voids have fundamental absorption in the UV range.[20]

UV-Vis spectrum of pure FLC (Fig. 5(b)) which consists of a mixture of two complex organic molecules, exhibits a broad and structureless absorption spectrum resulted from the superposition of absorption transitions arising from *p*-substituted biphenyl core bonded to long aliphatic terminal chain, isopropyl group, substituted ethylene, hetero nuclear nitrogen ring, nitrile, carboxylate ion, electron donating chlorine atom present in FLC.[28] The shift in UV absorption at 260 nm (onset region) and 340 nm (falling off region) to higher wavelength as compared to benzene ring UV spectrum with two primary bands at 184 and 202 nm and a secondary band at 255 nm may be attributed to increase in $\pi$ conjugation in *para*-substituted benzene ring, nitrogen atoms with unpaired electrons and electron donating chlorine atom. In addition to these, $n \rightarrow \pi^*$ transitions arising from non-bonding electrons of nitrogen, oxygen and chlorine may also shift peaks to higher wavelength depending upon their availability and concentration.

Based upon the characteristics absorption values noted from UV-Vis spectra, PL emission of $Nd_2O_3$ NPs were recorded at 205 nm, 248 nm and 292 nm excitation wavelengths and best response was observed at 248 nm wavelength as shown in Fig. 6. These emission spectra exhibit a series of emission peaks with maxima at ~345–397 nm (UV), ~425–475 nm (blue), ~545–560 (green) and ~613 (red) wavelength regions. The broad emission band in the UV region appears due to the singly ionized oxygen vacancies in $Nd_2O_3$ (ref. 20) by the radiative recombination of photo-generated hole with an electron occupying at the oxygen vacancy.[21] The origin of visible emission *i.e.* blue, green and red emissions has been attributed to the recombination of electrons in the shallow defect levels with the photo excited holes in valence band. The ultraviolet (UV) emission transitions arise from the $Nd^{3+}$ ion transition from $^4D_{3/2} \rightarrow {}^4I_{9/2}$ and $^2P_{3/2} \rightarrow {}^4I_{11/2}$ or $^4D_{3/2} \rightarrow {}^4I_{13/2}$ levels. The blue, green and red emission band appears from ($^4I_{9/2} \rightarrow {}^2P_{3/2}$, $^2K_{15/2}$), ($^4I_{9/2} \rightarrow {}^4G_{5/2}$, $^4G_{7/2}$) and ($^4I_{9/2} \rightarrow {}^2H_{11/2}$) transitions respectively.[29,30]

PL spectra of pure FLC at different excitation wavelengths ranging from 303 to 343 nm is presented in Fig. 7(a). Emission spectra are broad in nature and composed of three or four submerged components. Gaussian fit for the PL peak at 343 nm excitation shows four submerged components at 397, 451, 510 and 527 nm (Fig. 7(b)). First major peak at 399 nm occurred in all the excitations with maximum intensity at 343 nm excitation and highest intensity emission peak at 450 nm was observed at 303 nm excitation. The position of 399 nm emission peak remains same with change in excitation wavelength. This UV emission peak corresponds to the radiative relaxation of electrons from the lowest unoccupied molecular orbital (LUMO) to the highest occupied molecular orbital (HOMO) energy levels in the FLC.[17] While, the visible emissions in 450–510 nm range exhibit continuous red shift with gradual fall in intensity on increasing excitation wavelength. The red shift in emission spectra can be understood in terms of columnar aggregates formation between the two structural components of FLC. Aromatic rings of these components arrange themselves in such a manner that the intermolecular distance between them is in the range of their van der Waals radii. In PL spectrum, excited state of such columnar structure is red-shifted due to delocalization of excited wave function over several subunits/molecules within the stack of molecules and lowering of energy relative to the localized excited state wave function of their monomer unit.

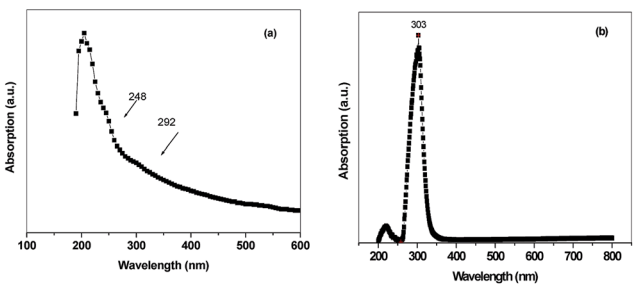


Fig. 5 UV-Vis absorption spectra of (a) $Nd_2O_3$ NPs and (b) FLC mixture ZLi 3654.

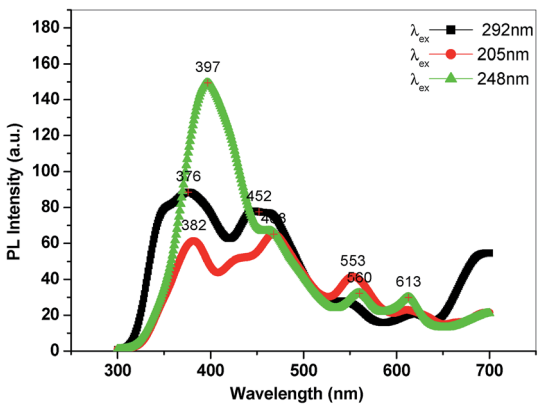


Fig. 6 Emission plots for the $Nd_2O_3$ NPs at different excitation wavelengths.

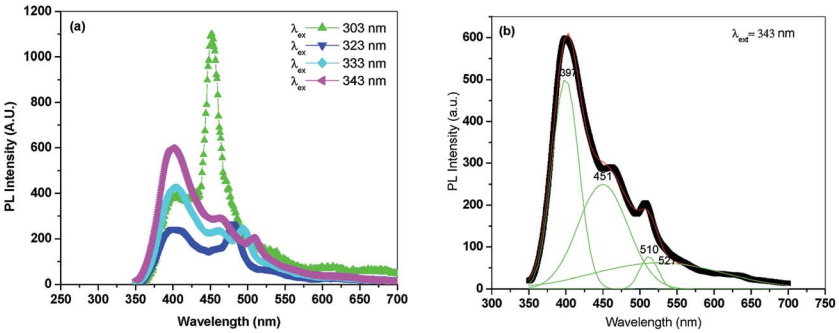


Fig. 7 (a) Emission plots for the FLC material at different excitation wavelengths, (b) Gaussian fit for the PL peak at 343 nm excitation shows four submerged components at 397, 451, 510 and 527 nm.

This kind of excitation wavelength dependence is not reported so far for ferroelectric liquid crystals.

PL spectra of FLC with $x$-$Nd_2O_3$ nanoparticles (NPs):FLC composites ($x$ = 2, 3, 5 and 8 μl) were recorded at different excitation wavelengths *i.e.* 248 nm (4.9994 eV), 303 nm (4.0919 eV), 323 nm (3.8385 eV) and 343 nm (3.6147 eV) to understand the effect of excitation wavelength on enhancement and quenching of PL emission and shift in their peak positions.

As shown in Fig. 8(a), PL spectra recorded at highest excitation energy *i.e.* at 248 nm showed enhancement in intensity of all emission peak without any blue or red shift with the increase in $Nd_2O_3$ NPs concentration in FLC. The peaks intensity enhancement with incorporation of $Nd_2O_3$ NPs in FLC matrix at 248 nm has been explained in terms of the introduction of more radiative levels in the host FLC by $Nd_2O_3$ NPs and easy transfer of energy from the emitted $Nd^{3+}$ ion photons to FLC host matrix to felicitate more transitions at this wavelength. The proposed mechanism for the PL peaks enhancement recorded at 248 nm has been demonstrated on the basis of up conversion mechanism for doped $Nd^{3+}$ ions: its ground state $^4I_{9/2}$ absorption excites electrons to higher $^2G_{5/2}$ excited state. The excited $Nd^{3+}$ ions relax non-radiatively to the metastable $^2H_{11/2}$ state and then re-excites to unstable $^4G_{11/2}$ level. The ion populated in $^4G_{11/2}$ either relax radiatively to different energy levels in visible region or transfers this excitation energy to liquid crystal molecules which resulted into the enhancement in PL emission intensity.

As shown in Fig. 9(a), at 303 nm excitation wavelength, PL spectra of pure FLC and (2, 5, 8 μl) $Nd_2O_3$ NPs:FLC nanocomposites give a weak peak at ~399 nm, very strong peak ~450 nm with very components at ~530 nm and ~670 nm. The intensity of these peaks reduces on increasing the $Nd^{3+}$ ions concentration in FLC matrix. The quenching in PL peaks is attributed to the disorder induced by the $Nd_2O_3$ NPs in FLC matrix and formation of non-radiative channels in the system. The cross relaxation process takes place by an efficient non-radiative electron transfer process from FLC to $Nd^{3+}$ because the host sensitized emissions have more efficient pathway than a direct excitation of $Nd^{3+}$ ions.[31,32]

A very similar quenching effect could also be seen at (Fig. 9(b)–(d)) higher excitation wavelength *i.e.* 323, 333 and 343 nm. In 323 nm excitation wavelength PL spectra of these samples, a broad absorption with strong peak at 401 nm in pure FLC which red shifts on adding $Nd_2O_3$ NPs in FLC and very strong peak at 484 nm. The broad emission bands arises from the quantum-confined excitonic states in FLC host and with shift in wavelength as compared to pure $Nd_2O_3$ NPs. This may be explained in terms of the change in population of $Nd^{3+}$ ions at different excited levels. In these spectra the red emission transitions are not observed. While in 343 nm excited wavelength, PL mission spectra of these samples show broad absorption with three peak maxima at ~360 nm, ~475 nm and ~530 nm in pure FLC and these peaks shift to higher wavelength in $Nd_2O_3$ NPs dispersed composites quenching in their

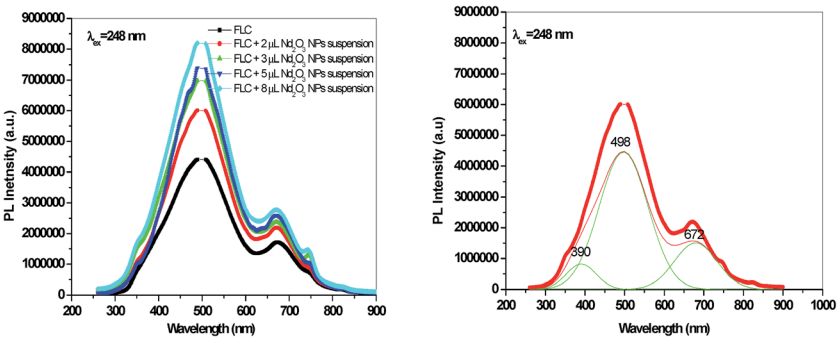


Fig. 8 (a) Emission response of FLC and their NPs doped analogues at 248 nm excitation (b) Gaussian fit for the PL emission peak shows three submerged components at 390, 498 and 672 nm.

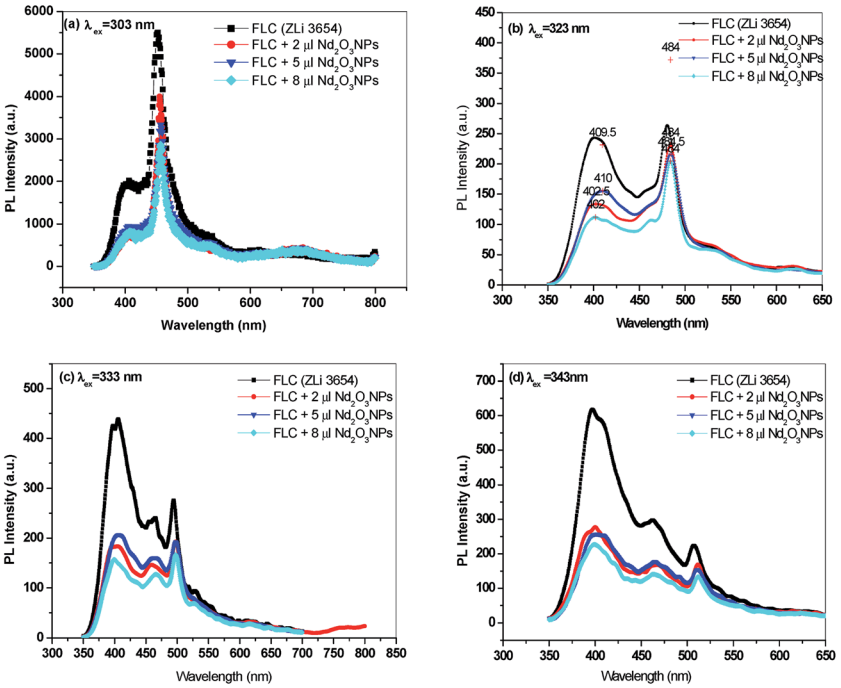


Fig. 9 Emission plots for FLC pure and $Nd_2O_3$ dispersed samples (a) $\lambda_{ext} = 303$ nm (b) $\lambda_{ext} = 323$ nm (c) $\lambda_{ext} = 333$ nm and (d) $\lambda_{ext} = 343$ nm.

intensity on increasing NPs concentration. In these spectra UV emission peak component at ~360 nm corresponds to the band gap absorption peak of FLC arising from near band edge emission *via* recombination of free exciton through an exciton–exciton collision process. The other components are observed in blue and green region of visible spectrum.

## Conclusion

Optical properties of $Nd_2O_3$ NPs dispersed ferroelectric liquid crystal (FLC) have been investigated by UV-Vis, PL and FTIR analytical techniques. IR transmittance spectra revealed the interaction of NPs with the long terminal groups of aromatic cored liquid crystal molecules whereas their inner core remains unaffected. The change in intensity and shift in peak positions of some bands have been attributed to change in crystalline field effect induced by the incorporation of $Nd_2O_3$ NPs in FLC matrix. The mechanism of enhancement and quenching in PL intensity of FLC–$Nd_2O_3$ nanocomposites at different excitation wavelength has been demonstrated from UV-Vis and photoluminescence (PL) studies. UV-Vis absorption spectra of $Nd_2O_3$ NPs shows two absorptions at 248 and 292 nm in the visible region whereas pure FLC has a broad absorption arising from the superposition of transitions from *p*-substituted biphenyl core bonded to different groups like long aliphatic terminal chain, isopropyl group, substituted ethylene, hetero nuclear nitrogen ring, nitrile, carboxylate ion, and electron donating chlorine atom *etc.* PL spectra of FLC with excitation wavelength dependence has been reported first time and the variations are explained in terms of the complex structure of FLC with various electron donating and withdrawing functional groups and hetero atoms with unpaired/non bonded paired electrons which create large number of defect levels in FLC band structure. PL emission of np-$Nd_2O_3$:FLC nanocomposites recorded at an excitation wavelength where $Nd_2O_3$ NPs show intense emission, *i.e.* 248 nm, exhibits an enhancement effect with gradually increasing the concentration of NPs upto 8 μl. While emission spectra at 303, 323, 333, 343 nm excitation wavelengths show a quenching of all the emission bands in FLC–NPs nanocomposites owing to the disorder caused by $Nd_2O_3$ NPs and creation of non-radiative channels in the system. These characteristics make these materials good candidates for applications in future organic electronic devices.

## Acknowledgements

The authors sincerely thank Director, IARI and Head, Agricultural Chemicals Division, IARI for continuous encouragement and interest in this work. Authors also wish to thank Sh. K. K. Somayajulu and Dr Suresh for FTIR characterizations. One of the authors (P. Goel) is also thankful to DST, New Delhi for financial support under INSPIRE Faculty Scheme (IFA12-PH-38).

## References

1 H. K. Bisoyi and S. Kumar, *Chem. Soc. Rev.*, 2011, **40**, 306.
2 I. Dierking, *Polym. Chem.*, 2010, **1**, 1153.
3 R. B. Meyer, L. Liebert, L. Strzelecki and P. Keller, *J. Phys., Lett.*, 1975, **36**, 69.
4 F. Fan, A. K. Srivastava, V. G. Chigrinov and H. S. Kwok, *Appl. Phys. Lett.*, 2012, **100**, 111105.
5 L. J. Yu and M. M. Labes, *Appl. Phys. Lett.*, 1977, **31**, 719.

6 C. Weder, C. Sarwa, A. Montali, C. Bastiaansen and P. Smith, *Science*, 1998, **279**, 835.
7 P. Goel and A. M. Biradar, *Appl. Phys. Lett.*, 2012, **101**, 074109.
8 A. Mikulko, P. Arora, A. Glushchenko, A. Lapanik and W. Haase, *EPL*, 2009, **87**, 27009.
9 Neeraj and K. K. Raina, *Opt. Mater.*, 2013, **35**, 531.
10 D. P. Singh, S. K. Gupta, S. Pandey, K. Singh and R. Manohar, *J. Appl. Phys.*, 2014, **115**, 214103.
11 R. Manohar, A. K. Srivastava, P. K. Tripathi and D. P. Singh, *J. Mater. Sci.*, 2011, **46**, 5969.
12 S.-Y. Huang, C.-C. Peng, L.-W. Tu and C.-T. Kuo, *Mol. Cryst. Liq. Cryst.*, 2009, **507**, 301.
13 S. Tripathi, P. Ganguly, D. Haranath, W. Haase and A. M. Biradar, *Appl. Phys. Lett.*, 2013, **102**, 063115.
14 A. Kumar, G. Singh, T. Joshi, G. K. Rao, A. K. Singh and A. M. Biradar, *Appl. Phys. Lett.*, 2012, **100**, 054102.
15 A. Kumar, J. Prakash, D. S. Mehta, A. M. Biradar and W. Haase, *Appl. Phys. Lett.*, 2009, **95**, 023117.
16 P. Ganguly, A. Kumar, S. Tripathi, D. Haranath and A. M. Biradar, *Appl. Phys. Lett.*, 2013, **102**, 222902.
17 P. Goel, M. Arora and A. M. Biradar, *RSC Adv.*, 2014, **4**, 11351.
18 A. Kumar, J. Prakash, A. D. Deshmukh, D. Haranath, P. Silotia, *et al.*, *Appl. Phys. Lett.*, 2012, **100**, 134101.
19 T. Lahiri, T. Pal Majumder and N. K. Ghosh, *J. Appl. Phys.*, 2013, **113**, 064308.
20 N. Salah, S. S. Habib, Z. H. Khan, S. A. Hamedi and S. P. Lochab, *J. Lumin.*, 2009, **129**, 192.
21 G. A. Kumar, C. W. Chen, J. Ballato and R. E. Riman, *Chem. Mater.*, 2007, **19**, 1523.
22 P. Goel, N. Vijayan and A. M. Biradar, *Ceram. Int.*, 2012, **38**, 3047.
23 R. M. Silverstein, F. X. Webster and D. J. Kiemle, *Spectrometric Identification of Organic Compounds*, John Wiley & Sons, Inc, 7th edn, 2005.
24 K. Ha and H.-J. Ahn, *Liq. Cryst.*, 2004, **31**, 1525.
25 S. Duhan, *Indian J. Pure Appl. Phys.*, 2009, **47**, 872.
26 S. Duhan, P. Aghamkar and M. Singh, *Res. Lett. Phys.*, 2008, 237023.
27 S. Surbhi, P. Aghamkar and S. Kumar, *Adv. Mater. Lett.*, 2013, **4**, 78.
28 P. S. Kalsi, *Spectroscopy of organic compounds*, New Age International, 6th edn, 01-Jan-2007, pp. 9–54.
29 B. Karthikeyan and S. Mohan, *Phys. B*, 2003, **334**, 298.
30 G. H. Dieke, *Spectra Energy Levels Rare-Earth Ions Cryst.*, Wiley Interscience, New York, 1968.
31 J. A. Caird, A. J. Ramponi and P. R. Staver, *J. Opt. Soc. Am. B*, 1991, **8**, 1391.
32 C. Jacinto, S. L. Oliveira, L. A. O. Nunes, M. J. Myers and T. Catunda, *Phys. Rev. B: Condens. Matter Mater. Phys.*, 2006, **73**, 125107.